We thank both reviewers for taking the time to review the manuscript again. We have responded to the comments from Reviewer 1 below with their comments in bold and our response in normal formatting. Reviewer 2 did not have comments to respond to.

Overall, the manuscript has become clearer and the authors have addressed most of my comments. However, some parts in Article and especially in Suppl. Material remain still unclear, as illustrated below. It is also confusing that the authors did not distinguish the figures in Suppl. Material (usually denoted as Figure S1, S2, etc.) from the figures in the main Article.

Thank you for highlighting this, unfortunately this was missed when originally compiling the supplementary material. The figures in the supplementary material are now labelled appropriately, e.g., Figure S1. We have also highlighted that these are found in the Supplementary material when referred to from the main article.

We have rearranged the order of Sections and Figures in the Supplementary material so that Figures are now grouped by subject for better clarity. We have also added an additional figure to the supplementary material (Figure S6) showing the comparison of CO_2 sensitivity when globally averaged that was removed from the main text in the previous revision but was still being referred to:

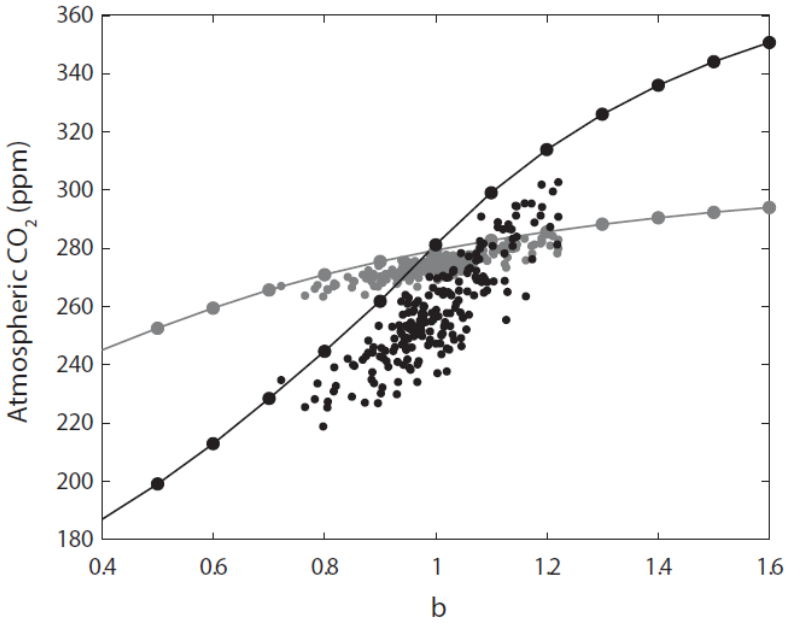

I appreciate the additional sensitivity experiments where atmospheric CO2 is explicitly simulated, instead of being inferred from preformed PO4 changes in the model. In the manuscript, the authors stated that atmospheric CO2 was explicitly simulated in the "global" sensitivity experiment (page 4, line 29-page 5, line 11) and that the relationship between preformed PO4 and atmospheric CO2 was derived from Figure A1. In Suppl. Material and the response letter, the authors also stated that atmospheric CO2 was also explicitly simulated in the regional sensitivity experiments and added Figure 1. From which figure do the authors derive the relationship between preformed PO4 and atmospheric CO2 when estimating the regional sensitivity of atmospheric CO2 to change in b from the Latin Hypercube ensemble?

Thank you for highlighting that this is not clear. The statistical relationship between atmospheric CO_2 and preformed PO_4 used in the Latin hypercube experiments is that shown in Figure A1. The regional sensitivity experiments in the Supplemental material are intended only to demonstrate the robustness of using the statistical relationship versus with an explicit carbon cycle. We note that since the relationships between atmospheric CO_2 and preformed PO_4 shown in Figure S1 do not deviate significantly from the global sensitivity runs, the statistical relationship would be very close.

We have updated the text in the supplementary material to explicitly state that the relationship in Figure A1 is used to infer atmospheric CO_2 from preformed PO_4 in the Latin hypercube experiments.

Likewise, it is difficult to understand the newly added Figures 1 though 3 in Suppl. Material. For example, what is the difference between Figure 1a and 1b, and between Figure 1c and 1d? What do the authors mean by "region of interest expanded"? Why do the relationships between preformed PO4 and atmospheric CO2 differ between Figure 1a (linear) and 1b (non-linear)?

We have added labels on Figure S1 to help distinguish that panels a & b correspond to the results obtained with the constant-export uptake scheme whilst panels c & d correspond to the nutrient-restoring scheme. These were also incorrectly stated in the caption and have been fixed.

The "region of interest" indicates that the bottom panels of Figure S1 are magnified axes of the data in the top panels to highlight the relatively small deviations from the global relationship. To make this clearer we have added boxes to the upper panels showing the extent of the axes in the lower panels and have labelled them to indicate the relevant panel.

The linear and non-linear relationships in Figure S1 reflect the behaviour of the model with either nutrient-restoring or constant-export schemes. They are the same relationships shown in Figure A1 which is already discussed in the second paragraph of the Results. We have added text to the caption of Figure S1 stating that panels a and c show the data from Figure A1 and have set the axis limits to the same as Figure A1 for clarity:

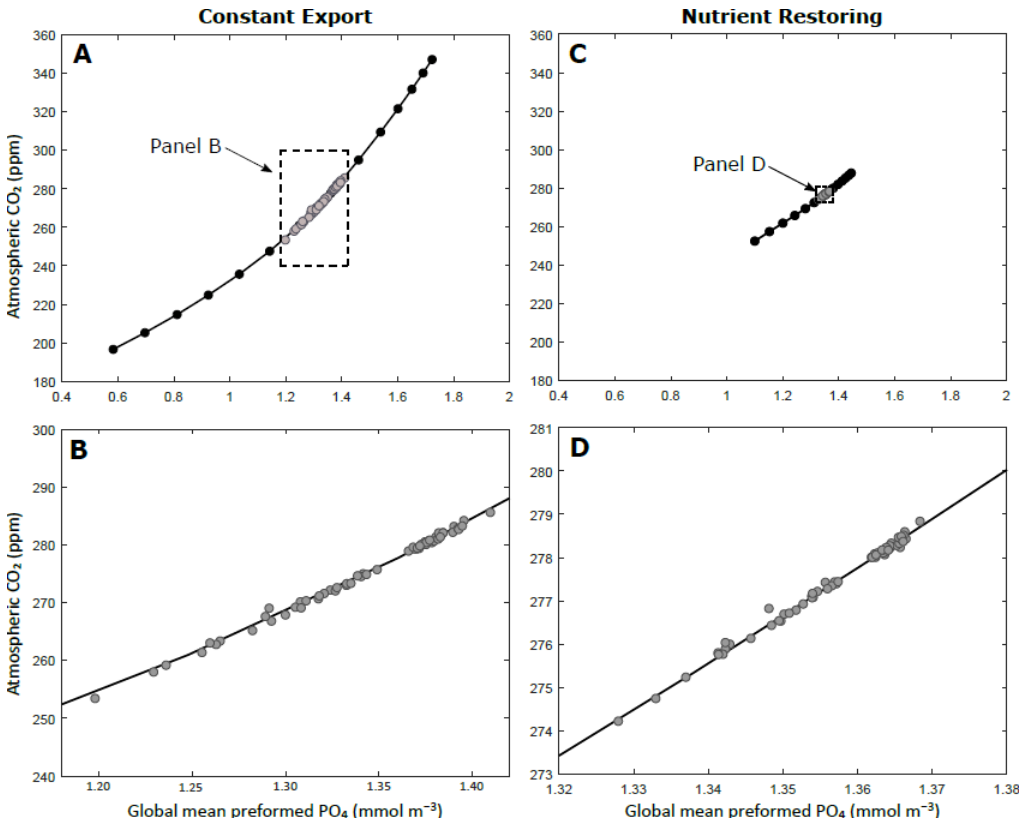

In Figure 2, the studentized residuals seem large, on the contrary to the residuals shown in Figure 1. Why?

The residuals in this figure are for the regression analysis that derives the sensitivity of atmospheric CO_2 to regional changes in b (Equation 2 in the main text).

We have added a reference to the equation in the figure caption and have changed the figure order to group the figures relating to the sensitivity evaluation together to aid clarity.

Which relationship is Figure 3 based on?

We have updated the caption to refer explicitly to descriptions of the experiments:

"Comparison of CO_2 sensitivity estimates from two methods. Black bars are the Latin hypercube and regression-based sensitivity estimates derived with the statistical relationship preformed PO_4 and CO_2 (Regional Sensitivity experiments described in Section 2.3 of the main text). Grey bars are the difference between CO_2 when each region is perturbed individually from b=0.4 and b=1.6 and atmospheric CO_2 is calculated explicitly in the model as described in Section 1 of the Supplementary material."

In Figure 3, the magnitudes of CO2 sensitivity look different between the black bars and the gray bars (not only for the absolute values but also for the relative values across the regions), although the authors claim that there is a good agreement. I feel that the authors need to discuss in what aspects the two (black vs. gray) do not agree and in what aspects the two agree in more details.

This figure previously showed the range of CO_2 across the individual perturbation experiments rather than the change in CO_2 per change in b which resulted in higher sensitivity estimates. The figure now shows sensitivity estimates based on the same method as the Latin hypercube estimates are more comparable:

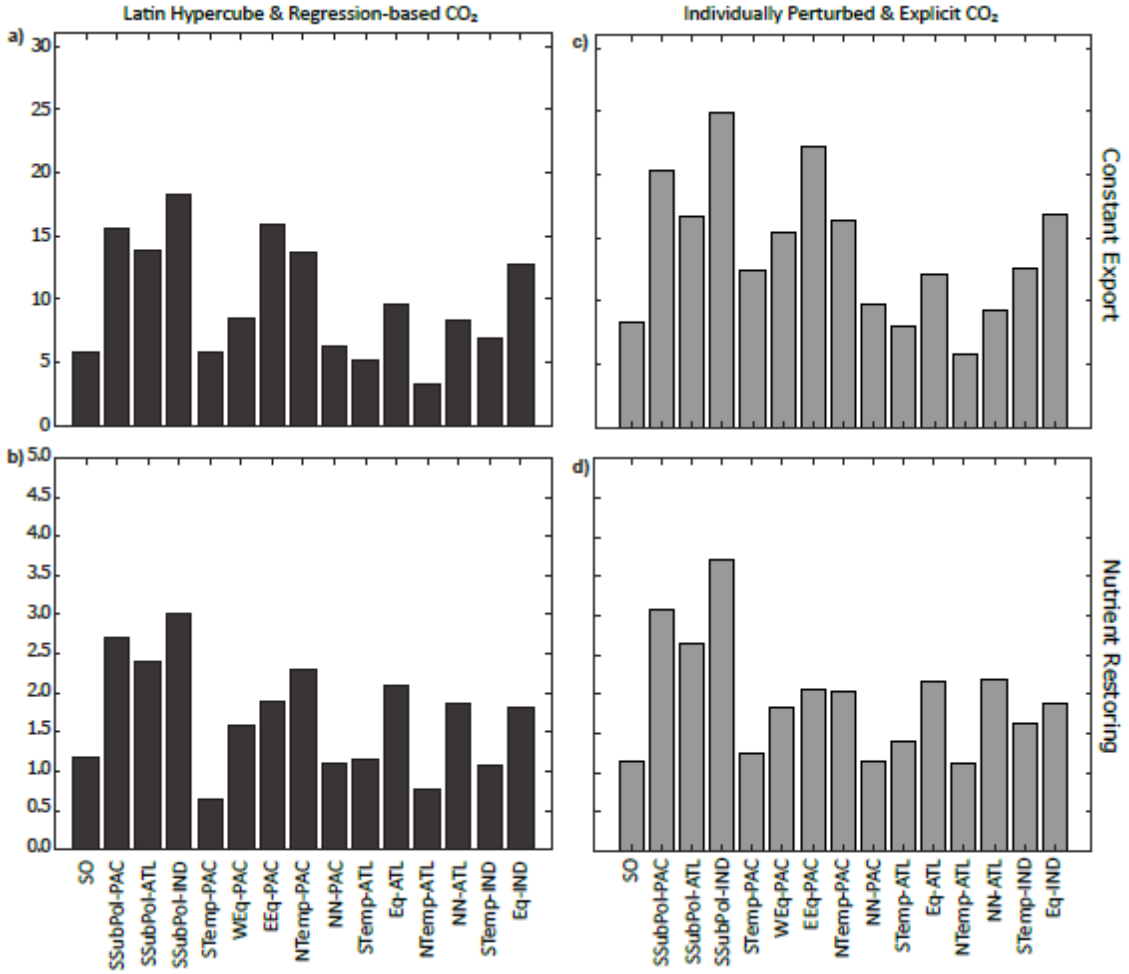

We have updated the text in the Supplementary material to briefly discuss the differences between the sensitivity estimates:

"The sensitivity estimates from the Latin hypercube ensemble (Figure 3 in the main text) are compared against the sensitivity of CO_2 from the individual 15 perturbation experiments with the explicit carbon cycle (Figure S2). The sensitivity of CO_2 is calculated in the same way as the Latin hypercube experiments using linear regression (eqn. 2 in the main text). The two estimates agree generally on the relative sensitivity between regions, e.g., there is a correlation coefficient of 0.94 between approaches for both the constant-export and restoring-uptake schemes. There are notable, but minor, differences between the sensitivity approaches. The Latin hypercube estimates are overall slightly lower for both export production schemes (Figures S2a & S2b cf. Figures S2c & S2d). Because the Martin curves are varied simultaneously in the Latin hypercube ensemble, this likely reflects that the sensitivity of CO_2 to the Martin curve in one region is offset by concurrent changes in other regions. However, the relative differences are preserved suggesting this is a minor effect. There are also minor changes in the relative sensitivity between regions. For example, the individual perturbation experiments predict that the STemp-IND region is more sensitive that the NN-ATL region for the constant-export model (Figure S2a cf. S2c), and that the NTemp-PAC region is less sensitive than the EEq-PAC region in the restoring-uptake model

(Figure S2b cf. S2d). These differences are within the 95% confidence intervals (Figure 3 in main text) and do not affect the key findings."

In Figure 3 and Table 1 of the main article, it would be useful if the authors can add the error bars for the regional CO2 sensitivity (e.g., the 95% confidence intervals for the regression coefficients). This can help to see how much the regional sensitivities discussed in this study are robust within the employed model framework.

We have added the 95% confidence intervals for the regression coefficients onto Figure 3 and Table 1:

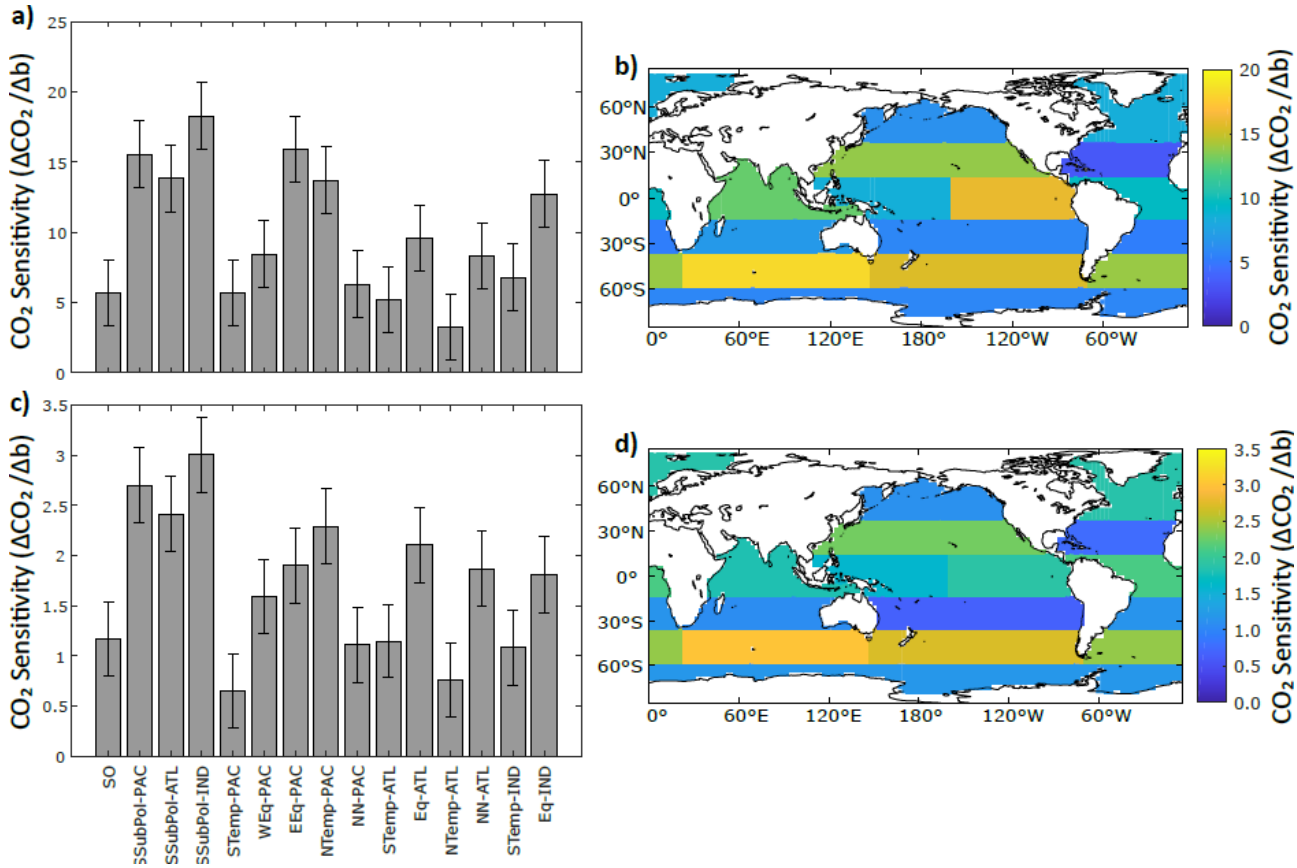

The revised Figure 5 and the associated text are clearer than before. However, I am still having difficulty in understanding the method and result. So, what is exactly plotted in Figure 5? Is it bkregion from Equation (3) (page 6, line 30)? Or is it bkregion from another equation where the Ppreregion in Equation (3) is replaced with the normalized Ppreregion? If the latter is true, then the "^" sign is missing in Ppreregion in page 7, line 4.

Thank you for highlighting that this was not clear enough. The reviewer is correct in stating that $\overline{[P_{pre}^{region}]}$ in equation 3 should be replaced with $\overline{[\widehat{P_{pre}^{region}}]}$. Equation 3 and the associated text in the manuscript has been updated to include this.

Page 3, Line 33: what do the authors mean by "a previous run"?

Changed to "fixed to that of the control run".

(Supplementary) Figure 2 y-axis labels: a typo in “Studenised”

Fixed.

(Supplementary) Figure 3 caption: a typo in “hyperube”

Fixed.

(Supplementary) Page2, line 1: a typo in “usedn”

Fixed.

Sensitivity of atmospheric CO_2 to regional variability in particulate organic matter remineralization depths

Jamie D. Wilson[1,2], Stephen Barker[2], Neil R. Edwards[3], Philip B. Holden[3], and Andy Ridgwell[1,4]

[1]BRIDGE, School of Geographical Sciences, University of Bristol, UK
[2]School of Earth and Ocean Sciences, Cardiff University, UK
[3]School of Environment, Earth and Ecosystems, Open University, UK
[4]Department of Earth Sciences, University of California, Riverside, USA

Correspondence: Jamie D. Wilson (jamie.wilson@bristol.ac.uk)

Abstract.

The concentration of CO_2 in the atmosphere is sensitive to changes in the depth at which sinking particulate organic matter is remineralised: often described as a change in the exponent "*b*" of the Martin curve. Sediment trap observations from deep and intermediate depths suggest there is a spatially heterogeneous pattern of b, particularly varying with latitude, but disagree over the exact spatial patterns. Here we use a biogeochemical model of the phosphorus cycle coupled with a steady-state representation of ocean circulation to explore the sensitivity of preformed phosphate and atmospheric CO_2 to spatial variability in remineralisation depths. A Latin hypercube sampling method is used to simultaneously vary the Martin curve indepedently within 15 different regions, as a basis for a regression-based analysis used to derive a quantitative measure of sensitivity. Approximately 30% of the sensitivity of atmospheric CO_2 to changes in remineralisation depths is driven by changes in the Subantarctic region (36°S to 60°S), simliar in magnitude to the Pacific basin despite the much smaller area and lower export production. Overall, the absolute magnitude of sensitivity is controlled by export production but the relative spatial patterns in sensitivity are predominantly constrained by ocean circulation pathways. The high sensitivity in the Subantarctic regions is driven by a combination of high export production and the high connectivity of these regions to regions important for the export of preformed nutrients such as the Southern Ocean and North Atlantic. Overall, regionally varying remineralisation depths contribute to variability in CO_2 of between $\pm$ 5 - 15 ppm relative to a global mean change in remineralisation depth. Future changes in the environmental and ecological drivers of remineralisation, such as temperature and ocean acidification, are expected to be most significant in the high latitudes where CO_2 sensitivity to remineralisation is also highest. The importance of ocean circulation pathways to the high sensitivity in Subantarctic regions also has significance for past climates given the importance of circulation changes in the Southern Ocean.

1 Introduction

Sinking particles of organic matter transfer 5-10 Pg C per year from the upper ocean to the ocean interior (Henson et al., 2011), as part of a process known as the biological pump. As these particles sink, they are remineralised through bacterial and zooplankton-related activity, releasing the carbon and nutrients back into solution at depth. Vertical fluxes of particulate

organic carbon (POC) in the water column have historically been described by the Martin Curve, a power-law function that describes the rapid decrease in flux (F_z) from a maximum value at depth z_0, nominally the base of the mixed layer, to a small asymptotic value in deep waters (equation 1: Martin et al., 1987) (Fig. 1):

$$F_z = F_{z_0} \left(\frac{z}{z_0} \right)^{-b} \tag{1}$$

The dimensionless exponent in the power-law ('b') describes whether organic matter is remineralised predominantly at shallower depths (larger values of b, e.g., b=1.6) or deeper in the water column (smaller values of b, e.g., b=0.4) (Fig. 1). The exponent itself parameterises the rate at which POC sinks through the water column (units of m day^{-1}) and the rate at which it is remineralised (units of day^{-1}) (Kriest and Oschlies, 2008; Lam et al., 2011). In this paper we use the term 'remineralisation depth', defined as a depth at which a defined % of POC has been remineralised. Previously, this has been defined as an *e*-folding depth: the depth at which $\sim$63% of POC has been remineralised (Kwon et al., 2009) (although note the Martin curve is not exponential).

Ocean biogeochemical models predict that the concentration of CO_2 in the atmosphere is sensitive to changes in a globally uniform remineralisation depth. Kwon et al. (2009) showed that a deepening of the remineralisation depth globally of 24 m (from b =1.0 to 0.9), redistributed dissolved inorganic carbon (DIC) from the intermediate waters to the deep ocean leading to a reduction in atmospheric CO_2 of between 10 and 27 ppm. The drawdown was also associated with a decrease in the global mean concentration of preformed nutrients in the ocean interior (nutrients that are not utilised by biology in the surface ocean and enter the ocean interior via circulation: Ito and Follows, 2005). Kwon et al. (2009) found that an increase in respired carbon in the deep ocean was balanced by a reduction in preformed nutrients exported in the North Atlantic. Deepening of the POC remineralisation depth could also drive dissolution of calcium carbonate ($CaCO_3$) in ocean sediments ultimately drawing down more CO_2 over millennial timescales (Roth et al., 2014). The potential impact of remineralisation depth changes on atmospheric CO_2 is therefore a highly relevant component of the marine carbon cycle for both past and current changes in climate (Riebesell et al., 2009; Hülse et al., 2017; Meyer et al., 2016).

Analyses of global sediment trap observations suggest there is a spatially heterogeneous pattern of remineralisation depths in the modern ocean that varies particularly with latitude. A synthesis of observations from deep sediment traps (>1500–2000 m: Henson et al., 2012) suggests that POC fluxes in high latitudes attenuate faster with depth (shallower remineralisation depth: b=1.6) than in low latitudes, where a greater proportion of POC is transported to depth (deeper remineralisation depth: b=0.4), (Fig. 1). However, POC fluxes measured using neutrally buoyant sediment traps at shallower depths (<1000 m) suggest the inverse of this latitudinal pattern (Marsay et al., 2015) (see also, Weber et al., 2016). A recent compilation of sediment trap data and profiles of particle size distributions observed in the water column highlight additional intra-basin variability in b (e.g., shallower remineralisation in the East Equatorial Pacific than in the West) and inter-basin variability (e.g., deeper remineralisation in the Atlantic and Indian basins compared to the Pacific) (Guidi et al., 2015). The uncertainty in the spatial variability of remineralisation depths presents a challenge for determining which mechanisms may be responsible for changes in remineralisation depths and how these might drive future or past changes in remineralisation (e.g., Boyd, 2015). Additionally,

this also presents a challenge for biogeochemical models that are beginning to resolve the mechanisms that are potentially responsible for these spatial patterns such as particle size dependent sinking rates (DeVries et al., 2014), temperature dependent remineralisation (John et al., 2014), and oxygen dependence (Laufkötter et al., 2017).

A key question in light of the observed spatial variability in remineralisation depths and the associated uncertainty in spatial patterns is: what is the sensitivity of atmospheric CO_2 concentrations to spatial variability in remineralisation depths? Kwon et al. (2009) further quantified the sensitivity of atmospheric CO_2 to basin scale changes in remineralisation depths by perturbing them in each basin individually, finding that the Pacific, Southern Ocean (defined as $>40°S$), Atlantic and Indian Oceans contributed 38%, 22%, 21% and 19% of the total CO_2 drawdown respectively (Kwon et al., 2009). The variability in CO_2 sensitivity between basins matched the variability in the magnitude of export production integrated over the basins and basin area, suggesting that no one region was more significant when varying the globally uniform remineralisation depth (Kwon et al., 2009). However, this basin-scale analysis does not resolve the sensitivity of atmospheric CO_2 occuring at the resolution suggested by observations, i.e., a latitudinal and within-basin scale, or at the resolution of ecological and biogeochemical variability (Longhurst, 1998; Fay and McKinley, 2014). Additionally the analysis does not allow for the identification of potential interactions and feedbacks between regions when remineralisation depths are changing simultaneously.

Here we aim to address these issues by performing a global sensitivity analysis of regionally varying remineralisation depths. To this end, we use a transport matrix (a steady-state computationally efficient representation of ocean transport) derived from the MIT global circulation model (MITgcm) with a model of phosphorus and carbon cycling where the ocean is divided into 15 regions in which remineralisation depths can change independently. Remineralisation depths are perturbed simultaneously using Latin hypercube sampling and sensitivity quantified using regression analysis,.

2 Methods

2.1 Model Description

We provide a brief description of the model here and a more detailed description in Appendix A. The approach to quantifying sensitivity used here relies on the ability to run an ensemble of model experiments. To make this approach feasible we use the 'transport matrix method' (Khatiwala et al., 2005; Khatiwala, 2007), a steady-state computationally efficient representation of ocean transport and climate derived from a global circulation model. We use monthly mean transport matrices derived from the 2.8° global configuration of the MIT global circulation model (MITgcm) with 15 vertical levels (Khatiwala et al., 2005; Khatiwala, 2007). These specific matrices have been previously applied to model biogeochemistry (Kriest et al., 2012; Kriest and Oschlies, 2015).

The biogeochemical model used here is a model of the marine phosphorus and carbon cycle that resolves phosphate (PO_4), dissolved organic phosphorus (DOP), dissolved inorganic carbon (DIC), total alkalinity and atmospheric CO_2. Following Kwon et al. (2009), we calculate the production of organic matter using either a nutrient-restoring scheme, where $[PO_4]$ is restored to monthly observations of $[PO_4]$ (Garcia et al., 2014) with a timescale of 30 days (eqn. A3), or with constant export production where export production is fixed to that of ~~a previous~~ the control run unless local nutrients fall below zero. These two schemes

represent two end-member scenarios, strictly within the context of this model, where organic matter production either depends entirely on macronutrient concentrations and can increase with higher nutrient fluxes (restoring) or is limited by other factors such as light or micronutrients (constant export). The remineralisation of particulate organic matter is parameterised using the Martin curve (eqn 1). To further facilitate a large number of experiments for the sensitivity analysis, we use the model to define a statistical relationship between preformed PO_4 (P_{pre}) and atmospheric CO_2 and run the model with a phosphorus cycle only (see Section A2.3).

2.2 Experiment Design

2.2.1 Defining Regions

We define a set of oceanic regions to approximately encapsulate the large-scale variability in biogeochemistry and patterns of remineralisation depths observed in sediment trap studies. We define regions by lines of latitude and basins, similar to the approach used by air-sea flux inversion studies, e.g., (Gloor et al., 2001; Mikaloff Fletcher et al., 2006). 15 regions are defined based on a partitioning by Gloor et al. (2001) with some minor changes (Fig. 2a). The assigned regions broadly correspond with major features in observed surface [PO_4] such as higher concentrations in upwelling regions and lower concentrations in the nutrient-depleted gyres (Fig. 2b). This suggests the regions should be a reasonable analogue for an alternative approach that captures key spatial variability in ecology and biogeochemistry by defining regions using vertical mixing, mixed layer depths, sea ice and sea surface temperature (Longhurst, 1998; Sarmiento et al., 2004; Henson et al., 2010; Fay and McKinley, 2014). The regions are also comparable to the ocean biomes defined in previous biological pump studies (e.g., Weber et al., 2016; Pasquier and Holzer, 2016).

2.3 Experiments

We perform a set of experiments to explore the sensitivity of atmospheric CO_2 to regional variability in b with the aim to quantitatively rank the sensitivity of atmospheric CO_2 to remineralisation depth changes in each region (e.g., Pianosi et al., 2016):

1. *Control Run*: A pre-industrial control run is set up with export production diagnosed by restoring to observed surface [PO_4], a globally uniform Martin exponent of 1.0 and initialised with globally uniform tracer concentrations. Atmospheric CO_2 is restored to 278 ppm. A globally uniform Martin exponent gives the lowest volume-weighted root mean square misfit compared to annual mean World Ocean Atlas 2013 [PO_4] observations (Garcia et al., 2014), as found in other studies using the same MITgcm transport matrices (Kriest et al., 2012). The control run is spun-up from uniform initial conditions for 5000 years.

2. *Global Sensitivity*: The Martin curve is varied globally, i.e., all regions are assigned the same exponent, between 0.4 and 1.6 in 0.1 increments, based on the range of spatial variability observed in the modern ocean (Henson et al., 2012;

Marsay et al., 2015; Guidi et al., 2015). Each experiment is run for 3,000 years continuing from the control run using the nutrient-restoring scheme to predict export production (eqn. A3) and freely evolving atmospheric CO_2.

3. *Regional Sensitivity*: Latin hypercube sampling, a stratified-random procedure that provides an efficient way of sampling high dimensional parameter space (McKay et al., 1979), is used to vary the Martin curves in every region simultaneously.. Values of b are sampled from a uniform distribution ranging from 0.4 to 1.6 using the 'lhsdesign' function in MATLAB with 'maximin' sampling (an additional constraint that helps reduce clustering of samples, by maximising the minimum distance between points, in order to give a well-spread distribution of points across the parameter space). The range of b used centres around b=1.0 as used for the control run. We generate a Latin hypercube ensemble with 200 experiments, balancing the need for higher sampling resolution of the parameter space and total computational time. Each experiment is run for 3000 years continued on from the control run with a phosphorus cycle only. Changes in atmospheric CO_2 are inferred from changes in preformed PO_4.

Both the global and regional sensitivity experiments are repeated with constant-export production that is diagnosed from the control run. All output is diagnosed from the last full simulation year.

2.4 Sensitivity Analysis

We use multiple linear regression analysis to derive the sensitivity of atmospheric CO_2 to changes in b in each region (k) where the fitted coefficients (β_k) give a quantitative measure of the sensitivity (e.g., Pianosi et al., 2016):

$$CO_2 = \beta_0 + \sum_k \beta_k b_k \tag{2}$$

3 Results

3.1 Sensitivity of CO_2 to regional variability in remineralization depths

To quantify the sensitivity of CO_2 to regional changes in b we fit linear regression models (eqn 2) to the results of the Latin hypercube ensembles. The resulting regression models explain a large proportion of the variability between CO_2 and b (R^2 = 0.88 and 0.90 for the constant-export and restoring-uptake ensembles respectively). Residuals of the regression models showed no significant bias versus the regression output (Fig. ~~S2~~S5 in Supplementary) suggesting that a linear model was appropriate. Although the relationship between CO_2 and a globally-uniform remineralisation depth is non-linear (e.g., Fig. 6), the relationship is near linear around the observed global mean in the centre of the range of b tested (see also, Kwon et al., 2009). Overall, the absence of a strongly non-linear relationship suggests the use of a linear regression model is appropriate (Pianosi et al., 2016).

When b is varied as a globally uniform parameter from 0.4 to 1.6, atmospheric CO_2 varies from 197 to 347 ppm (range of 150 ppm) for the constant-export scheme and from 257 to 288 ppm (range of 31 ppm) for the nutrient-restoring scheme, consistent

with previous model experiments (Kwon et al., 2009). Figure 3 shows how the sensitivity of CO_2 to changes in b varies as a function of region. CO_2 is most sensitive to changes in b occuring in the Subantarctic regions, with CO_2 being most sensitive to changes in the Indian sector of the Subantarctic (Fig. 3, Table 1). The Southern Ocean and sub-tropical gyres, with the exception of the gyre in the North Pacific, are consistently the regions where b has the smallest impact on CO_2. Other regions, including the equatorial Indian ocean, Equatorial Pacific and North Pacific have an intermediate sensitivity. As a region, the Subantarctic is responsible for $\sim$30% of the CO_2 sensitivity, comparable to the Pacific basin-scale sensitivity (Table 1).

As with the globally uniform changes in b, the magnitudes of regional sensitivities are smaller when run with nutrient-restoring uptake as opposed to a constant-export scheme because export production is able to convert any increase in surface nutrient and carbon fluxes back into organic matter, limiting any change in CO_2 fluxes. However, the relative sensitivity ranked across regions remains similar, as shown by expressing β_k as a percentage of $\sum_k \beta_k$ (Table 1). Therefore, the regional patterns in Figure 3 are not sensitive to assumptions about the response of nutrient uptake to the redistribution of nutrients. This suggests whilst the absolute magnitude of CO_2 sensitivity to changes in b is related to global export production it is not driven by local changes in export production specific to any region(s).

Kwon et al. (2009) demonstrated that the sensitivity of CO_2 to basin-scale changes in b correlated with the magnitude of export production in each basin. Similarly, we find a general positive correlation between sensitivity and regional export production (r=0.79, p$<$0.01 for constant export, r=0.47, p=0.07 for restoring uptake), as measured by the mean annual average export production across the 200 ensemble runs (Fig 4). The correlation is much weaker with nutrient-restoring uptake compared to the constant-export production. Intuitively, regions with lower export production, i.e., that contribute less to the inventory of regenerated PO_4, have a smaller impact on the balance between preformed and regenerated nutrients and therefore on atmospheric CO_2. Whilst CO_2 is generally more sensitive to remineralisation depths in regions with higher export production, sensitivity varies across regions with similar export production. For example, the sensitivity for the temperate North Pacific (NTemp-PAC; Fig. 4a) ($\Delta CO_2/\Delta b$ = 13.72, export production = 1.4$\pm$0.11 Tmol P year^{-1}) is approximately double that of the sub-polar region of the Southern Pacific (STemp-PAC; Fig. 4a) ($\Delta CO_2/\Delta b$ = 5.72, export production = 1.4$\pm$0.17 Tmol P year^{-1}). There are no apparent relationships between the variability of export production across the ensemble in each region, as shown by the horizontal errorbars, and sensitivity (Fig. 4). This further supports the finding that the response of export production to changes in nutrient distributions are not an important factor in the sensitivity of CO_2 to regional changes in b.

The variability in sensitivity not explained by the magnitude of POC export is likely a function of how changing remineralisation depths interact with ocean circulation. To quantify this effect we calculate the mean preformed PO_4 in the ocean interior derived from each region individually ($\overline{[P_{pre}^{region}]}$) (see Appendix A2.3) and repeat the sensitivity regression analysis. In order

to compare regression coefficients from different regions with significantly different magnitudes of $\overline{[P^{region}_{pre}]}$ we first normalise the concentrations ($\overline{[P^{region}_{pre}]}$) to the range of variability across the 200 experiments:

$$\hat{\overline{[P^{region}_{pre}]}} = \beta^r_0 + \sum_k \beta^{region}_k b_k \frac{\overline{[P^{region}_{pre}]} - \min(\overline{[P^{region}_{pre}]})}{\max(\overline{[P^{region}_{pre}]}) - \min(\overline{[P^{region}_{pre}]})} \quad (3)$$

The new regression analysis (eqn. 4) now predicts the contribution of changing b in all regions to the change in ~~$\overline{[P^{region}_{pre}]}$~~ $\hat{\overline{[P^{region}_{pre}]}}$ derived from a single region rather than globally (Fig. 5).The regression analysis is repeated for each region~~but the mean concentration of preformed PO_4 derived from each region varies by up to four orders of magnitude between different regions. In order to compare regression coefficients from different regions we first normalise the concentrations ($\hat{\overline{[P^{region}_{pre}]}}$) to the range of variability across the 200 experiments:~~.

$$\hat{\overline{[P^{region}_{pre}]}} = \beta^r_0 + \sum_k \beta^{region}_k b_k \quad (4)$$

Figure 5 shows the relative sensitivity of ~~$\overline{[P^{region}_{pre}]}$~~ $\hat{\overline{[P^{region}_{pre}]}}$ to changes in b. R^2 ranges from 0.82 to 0.97 suggesting overall the linear regression models are appropriate. The regression coefficients specific to a single region are collected from across the 15 regression results in each column of Figure 5. By definition, each row of Figure 5 shows the effect of changing b in the corresponding region on ~~$\overline{[P^{region}_{pre}]}$~~ $\hat{\overline{[P^{region}_{pre}]}}$ from all other regions.

The sensitivity analysis for each region on an individual basis shows that changes in b in the Subantarctic regions have large impacts on ~~$\overline{[P^{region}_{pre}]}$~~ $\hat{\overline{[P^{region}_{pre}]}}$ across regions globally (Fig. 5). In particular, these regions have a particular effect on the ~~$\overline{[P^{region}_{pre}]}$~~ $\hat{\overline{[P^{region}_{pre}]}}$ export in the Southern Ocean and in the Atlantic as a basin, comparable in magnitude to the local changes in ~~$\overline{[P^{region}_{pre}]}$~~$\hat{\overline{[P^{region}_{pre}]}}$. Changes in b in the equatorial upwelling regions of the Pacific and Indian Oceans also have a large global effect but with a more pronounced local effect. These features are more pronounced with nutrient-restoring uptake (Fig. 5b). The Southern Ocean and North Atlantic regions are those with the highest ~~$\overline{[P^{region}_{pre}]}$~~ $\hat{\overline{[P^{region}_{pre}]}}$ export across the ensemble (Table 1), consistent with previous findings about the global importance of these regions for preformed PO_4 (DeVries et al., 2012; Pasquier and Holzer, 2016). This suggests the larger sensitivity of CO_2 to changes in b in the Subantarctic regions is due to the way in which the ocean circulation connects these regions to the Southern Ocean and North Atlantic. In contrast, changing b in the Southern Ocean and North Atlantic has a relatively minimal effect on ~~$\overline{[P^{region}_{pre}]}$~~ $\hat{\overline{[P^{region}_{pre}]}}$ (and by inference CO_2) both locally and globally.

3.2 Regional versus Global Sensitivity

Lastly, we explore whether the spatial patterns in sensitivity (Fig. 3) are significant on a global scale. Global average values of b are calculated for each of the 200 Latin hypercube samples using an area-weighted mean and compared against experiments where b is pertubed uniformly across regions (Fig. 6). The amount of organic matter reaching the deep ocean is a non-linear

function of b, following from the fact that the Martin curve represents the scenario of a fixed remineralisation rate and an increasing sinking rate (Kriest and Oschlies, 2008; Cael and Bisson, 2018) (see Supplementary Material). Therefore, larger values of b, i.e., shallower remineralisation, have disproportionally more weight when calculating a global arithmetic mean of spatially variable b values ~~.~~(Fig. S6). To account for this, we find the equivalent e-folding depths for each Latin hypercube sample, which form a skewed distribution due to higher occurrence of shallower remineralisation, calculate the area-weighted geometric mean e-folding depth for each sample, and re-arrange again for b (see Supplementary Material for details).

The relationship between CO_2 and the globally averaged b values from the sensitivity experiments closely matches the relationship between CO_2 and globally uniform b for the both constant-export and restoring uptake schemes (Fig. 6). Note that b in each region is varied within the full parameter range but that because Latin hypercube sampling varies all parameters across their parameter range simultaneously the global mean does not reach the highest and lowest global b values. The average regionally varying b values vary within $\sim \pm 15$ ppm of the globally uniform experiments with constant-export and $\sim \pm 5$ ppm for the nutrient-restoring experiments, comparable to the change in CO_2 for a globally uniform change in b of $\sim$0.2.

4 Discussion

Sediment trap observations reveal significant spatial variability in remineralisation depths. Here we have quantified the sensitivity of atmospheric CO_2 to regional changes in remineralisation depths and show that CO_2 is most sensitive to changes in the Subantarctic regions. Much of the observed spatial variability varies across latitudes (Henson et al., 2012; Guidi et al., 2015; Marsay et al., 2015; Weber et al., 2016). Additionally, the mechanisms potentially driving these patterns are also likely to vary on a latitudinal basis, with changes in related environmental properties in response to anthropogenic CO_2 emissions affecting the high latitudes in particular: temperature changes (Kirtman et al., 2013) affecting temperature-dependent remineralisation rates; a reduction in carbonate saturation state with ocean acidification (Orr et al., 2005) affecting ballasting and changes in plankton community composition; and cell size (Lefort et al., 2015) affecting aggregation dynamics and particle sinking velocities. Additionally, this is a consideration for changes in remineralisation depths occurring in past climates (Meyer et al., 2016). This suggests that the spatial patterns in CO_2 sensitivity could be significant when considering the impact of remineralisation depth changes.

Changes in the air-sea balance of carbon are commonly related to changes in preformed nutrients. Because of the inefficient utilisation of upwelled nutrients in the Southern Ocean this region has been identified as key to setting the efficiency of the biological pump (Ito and Follows, 2005; DeVries et al., 2012). Our results show that this is also key for the the sensitivity of CO_2 to regional variability in remineralisation depths because of upwelling in the Subantarctic regions (Fig. 5). This relationship has implications when invoking changes in the efficiency of the biological pump in past climates such as the Last Glacial Maximum (LGM). Processes that increase the utilisation of nutrients in the Southern Ocean, such as iron fertilisation, and processes that reduce the delivery of nutrients to the Southern Ocean, such as increased stratification, have been implicated in the drawdown of atmospheric CO_2 during the LGM (Sigman et al., 2010). Any changes in strafication will also impact the sensitivity of CO_2 to any additional changes in remineralisation depths, such as from changes in ballasting minerals and/or

temperature dependent remineralisation (Chikamoto et al., 2012). In comparison, processes such as iron fertilisation will not impact on this sensitivity. Because the spatial patterns of CO_2 sensitivity to regional changes in remineralisation are predominantly constrained by ocean circulation pathways, this also suggests that the sensitivity may change with a reorganisation of ocean circulation as suggested for the LGM (Sigman et al., 2010).

The Martin curve is a commonly used parameterisation of the remineralisation of particulate organic matter with depth in marine biogeochemical models, and is commonly applied with a globally uniform exponent (b) (Hülse et al., 2017). However, the Martin curve used in this way has potential limitations: it is an empirical and static parameterisation that does not represent the mechanisms affecting remineralisation and sinking rates; and it does not capture spatial variability in remineralisation observed in sediment trap data (Henson et al., 2012; Marsay et al., 2015; Guidi et al., 2015). In our sensitivity analysis, we have shown that CO_2 has a similar sensitivity to the global mean change in b as compared to a globally uniform change in b with an uncertainty of $\pm$5 - 15 ppm, equivalent to a change in b of $\sim$0.2 (Fig. 6). Kwon et al. (2009) suggest a decrease of 0.3 from the modern remineralisation depth is sufficient to explain the increase in deep ocean nutrient concentrations during the Last Glacial Maximum. For the 21st century, ~~(Laufkötter et al., 2017)~~ Laufkötter et al. (2017) predict a decrease of POC export at 500 m by 2100 under RCP8.5 in response to temperature and oxygen-dependent remineralisation, equivalent to a decrease in b of $\sim$0.25. As such, the global mean change in potential future and past changes in remineralisation depth may be larger than the uncertainty associated with spatial variability. This has potentially useful implications for modelling the remineralisation of particulate organic matter fluxes. Models resolving the various processes that affect remineralisation rates and sinking velocities have recently been developed (Jokulsdottir and Archer, 2016; Cram et al., 2018) however, the requirements to model processes such as particle aggregation can be computationally expensive, limiting their application to 1-D models (Jokulsdottir and Archer, 2016; Cram et al., 2018) or to offline models (DeVries et al., 2014). A globally uniform change in b informed by these models could then be used to calculate the impact on atmospheric CO_2 if the change in b is greater than 0.2. However, we note that the modern global mean b is subject to uncertainty associated with under-sampled spatial variability.

Our results are dependent on the use of transport matrices derived from one global circulation model. Whilst this model has been widely applied to study biogeochemistry previously, it is subject to a number of caveats. The ocean model predicts significantly larger outcrops of dense water in the Southern Ocean compared to observations ~~(see Figure S4 Duteil et al., 2013)~~ (see Figure S3 in S to deep-water formation occurring at latitudes around 50°S (Figure ~~S5~~S4 in Supplementary). The volumetric fraction of water in the ocean interior derived from the Subantarctic is also higher (26%) compared with data-constrained estimates ~~(18%: Khatiwala et al., 2012)~~(18%, Table S1: Khatiwala et al., 2012). As such, the sensitivity estimates for the Subantarctic may be over-estimated. This is also consistent with the higher sensitivity compared to the basin-scale analysis of Kwon et al. (2009) who found that the Southern Ocean (>40°S contributed 22% of the global CO_2 sensitivity, compared with 36% in this study (>38°S, Table 1). However, our results have key similarites, including absolute and relative magnitudes of regional preformed PO_4 export, to other studies using alternative steady-state circulation states (DeVries et al., 2012; Pasquier and Holzer, 2016). As such, our results should be broadly reproducible with other models. A disadvantage to using a steady-state circulation is that we cannot quantify impact of the CO_2-climate feedback on ocean circulation and atmospheric CO_2. Studies exploring the simultaneous effects of warming temperatures on circulation and biology in response to anthropogenic CO_2 emis-

sions show that changes in circulation could be as important as biological changes (Cao and Zhang, 2017), (but see, Yamamoto et al., 2018). Quantifying the regional sensitivity with a dynamic ocean is therefore an important focus for future work. Ratios of $CaCO_3$ to POC vary latitudinally, and could also therefore modify our sensitivity results. Segschneider and Bendtsen (2013) found important feedbacks involving interactions between calcifiers and silicifiers in an marine ecosystem model when exploring temperature dependent remineralisation rates in the 21st Century. Future model experiments including a representation of plankton ecosystems would therefore help explore the impact of $CaCO_3$ export on regional sensitivity patterns.

5 Conclusions

We have presented a sensitivity analysis that quantifies the sensitivity of atmospheric CO_2 to regional variability in particulate organic carbon remineralisation depths. CO_2 is most sensitive to changes in remineralisation depths occurring in the Subantarctic regions, particularly the Indian Sector. As a whole, the Subantarctic regions have a sensitivity similar to that of the Pacific basin despite the smaller area and levels of production. Sensitivity patterns are in part a function of the magnitude of export production in each region and the physical circulation pathways specific to each region. Whilst the overall magnitude of CO_2 sensitivity to regional changes is dependent on the magnitude and response of export production to changes in nutrients, the relative spatial patterns in sensitivity are predominantly constrained by ocean circulation pathways. We also find that the regional variability adds $\pm$5 - 15 ppm uncertainty to global mean changes in remineralisation depths. The regional patterns in sensitivity could be significant if a number of processes that potentially drive changes in remineralisation depths, including temperature-dependent remineralisation rates and plankton community structure, vary predominantly in the high latitudes. However, this uncertainty is similar to the change in CO_2 for a globally uniform change in b of $\sim$0.2 meaning that larger changes in b could be reliably approximated by a globally uniform b as commonly used in biogeochemical models.

Code and data availability. The transport matrices are publicly available at: http://kelvin.earth.ox.ac.uk/spk/Research/TMM/TransportMatrixConfigs. The model code is freely available at: http://github.com/JamieDWilson/FML

Appendix A: Model Description

The Latin hypercube sampling approach used relies on the ability to run an ensemble of model experiments. To make this approach feasible we use the 'transport matrix method' (Khatiwala et al., 2005; Khatiwala, 2007). The model is written in Fortran 90 and achieves $\sim$1500 years hour^{-1} on a single core.

A1 Steady-state Ocean Circulation Model

The matrix used here is the 2.8° global configuration of the MIT model with 15 vertical levels driven by seasonally cycling fluxes of momentum, heat, and freshwater, publicly available from http://kelvin.earth.ox.ac.uk/spk/Research/TMM/TransportMatrixConfigs

Seasonally varying ocean circulation is calculated at each timestep by linearly interpolating between monthly mean matrices. An advantage of using transport matrices is that the timestep can be made longer to reduce computational expense (Khatiwala, 2007). Here we extend the circulation timestep to 3.8 days.

A2 Biogeochemical Model

The biogeochemical model represents the cycle of phosphorus and carbon in the ocean with four dissolved tracers, PO_4, dissolved organic phosphorus (DOP), dissolved inorganic carbon (DIC) and total alkalinity. The biogeochemical model has the same timestep as the ocean circulation model (3.8 days).

A2.1 Phosphorus Cycle

PO_4 and DOP are governed by the following equations:

$$\frac{\mathrm{dPO_4}}{\mathrm{d}t} = \mathbf{A}\mathrm{PO_4} - J_{\mathrm{up}} + J_{\mathrm{POP}} + J_{\mathrm{DOP}} \tag{A1}$$

$$\frac{\mathrm{dDOP}}{\mathrm{d}t} = \mathbf{A}\mathrm{DOP} + v \cdot J_{\mathrm{up}} - J_{\mathrm{DOP}} \tag{A2}$$

where $\mathbf{A}$ denotes the transport matrix calculation of ocean transport and J denotes biogeochemical source/sink terms.

The uptake of PO_4 during production of organic matter occurs in the euphotic zone, here defined as the base of the upper two grid-boxes (120 m). Following Kwon et al. (2009) we calculate the production of organic matter using either a nutrient-restoring scheme or a constant-export scheme. The nutrient-restoring scheme restores surface concentrations of PO_4 to observed [PO_4] with a restoring timescale (τ = 30 days Najjar et al., 2007) and is scaled by the fraction of seaice present (F_{seaice}, as monthly average fields from the original global circulation model):

$$J_{\mathrm{up}} = \frac{1}{\tau} \max\Big(\big(\mathrm{PO_4} - \mathrm{PO_{4,}}_{obs}\big), 0\Big)(1 - F_{seaice}) \tag{A3}$$

Organic matter production in the constant-export scheme is fixed to that of the experiment defined as the control run unless surface [PO_4] is depleted below zero in which case J_{up} is set to zero at that timestep. The control run is defined as having the run with the lowest root mean square misfit compared to annual mean World Ocean Atlas [PO_4] observations.

A fixed fraction (v=0.66) of the organic matter production integrated across the upper two grid-boxes is routed directly to dissolved organic phosphorus (DOP) and remineralised back to PO_4 in a first-order reaction with decay rate κ throughout the water column:

$$J_{\mathrm{DOP}} = \kappa \mathrm{DOP} \tag{A4}$$

The remaining fraction of organic matter production ($(1-v$=0.34) is integrated across the upper two grid-boxes and exported as particulate organic phosphorus (POP) at the base of the of the second grid-box in the vertical (120 m). The remineralisation of POP is parameterised with the Martin Curve (Equation 1). POP that has reached the sediment is remineralised fully in the lowermost grid-box of the water column, maintaining a closed system with respect to [PO_4]. As such, there is no sediment component in this model.

A2.2 Carbon Cycle

The uptake of nutrients and remineralisation of particulate and dissolved organic phosphorus are related to dissolved inorganic carbon and alkalinity via Redfield ratios of 1:16:116 (P:N:C). Carbonate chemistry parameters are computed from dissolved inorganic carbon and alkalinity using the method described by Follows et al. (2006). The method provides a simplified but accurate solution with computational efficiency. The air-sea gas exchange of CO_2 is calculated as per Orr et al. (2017).

A2.3 Preformed PO_4 and atmospheric CO_2

Changes in atmospheric CO_2 due to changes in the biological pump can be directly related to the inventory or average concentration of preformed PO_4 (P_{pre}) if total nutrient concentrations are conserved (Ito and Follows, 2005; Marinov et al., 2008). This provides a way of relating changes in our model of the phosphorous cycle to changes in atmospheric CO_2 without simulating a relatively computationally expensive carbon cycle. The distribution of annual mean [P_{pre}] for each run is calculated by splitting the transport matrices into "interior" matrices ($\mathbf{A^I}$) and "exterior" matrices ($\mathbf{B}$) for both the explicit and implicit matrices (subscripts e and i respectively) (see Khatiwala, 2007). The annual mean surface [PO_4] from the end of a simulation is set as a boundary condition and solving for the interior distribution of P_{pre}:

$$\mathbf{P}_{\text{pre}} = (\mathbf{A_i^I A_e^I} - \mathbf{I})^{-1}((\mathbf{A_i^I B_e} + \mathbf{B_i})\mathbf{PO_4}) \tag{A5}$$

The global mean concentration of of P_{pre} ($\overline{[P_{pre}]}$) is related to CO_2 using a empirical quadratic function (eqn. A6) fitted to a series of experiments where the Martin curve is varied globally (see below). The function is derived from a non-linear least squares regression (Fig. A1). The resulting regression fit (details in Figure caption) is used to estimate changes in CO_2:

$$CO_2 = (\beta_1 \overline{[P_{pre}]}^2 + \beta_2 \overline{[P_{pre}]} + \beta_3) \tag{A6}$$

The approach to predict CO_2 from regional changes in b is evaluated in the Supplementary material and shows the approach is robust to factors such as the slow timescale for the air-sea gas exchange of CO_2 (e.g., Eggleston and Galbraith, 2018).

Author contributions. JDW designed the experiments, developed the model code and ran the model. JDW prepared the manuscript with input from all co-authors.

Competing interests. The authors declare that they have no conflict of interest.

Acknowledgements. This work is based on work originally conducted as part of a PhD project (JDW) associated with the UK Ocean Acidification Research Programme (UKOARP), grant NE/H017240/1 to AR and SB. JDW and AR acknowledge support via the EU grant ERC-2013-Cog-617313. We would like to thank Andrew Yool for his comments on an earlier version of the manuscript. We also thank Samar Khatiwala for making transport matrices freely available.

References

Boyd, P. W.: Toward quantifying the response of the oceans' biological pump to climate change, Frontiers in Marine Science, 2, 77, https://doi.org/10.3389/fmars.2015.00077, http://journal.frontiersin.org/article/10.3389/fmars.2015.00077, 2015.

Cael, B. B. and Bisson, K.: Particle Flux Parameterizations: Quantitative and Mechanistic Similarities and Differences, Frontiers in Marine Science, 5, 395, https://doi.org/10.3389/fmars.2018.00395, https://www.frontiersin.org/article/10.3389/fmars.2018.00395, 2018.

Cao, L. and Zhang, H.: The role of biological rates in the simulated warming effect on oceanic CO_2 uptake, Journal of Geophysical Research: Biogeosciences, 122, 1098–1106, https://doi.org/10.1002/2016JG003756, http://dx.doi.org/10.1002/2016JG003756, 2017.

Chikamoto, M. O., Abe-Ouchi, A., Oka, A., and Smith, S. L.: Temperature-induced marine export production during glacial period, Geophysical Research Letters, 39, L21 601, https://doi.org/10.1029/2012GL053828, http://dx.doi.org/10.1029/2012GL053828, 2012.

Cram, J. A., Weber, T., Leung, S. W., McDonnell, A. M. P., Liang, J.-H., and Deutsch, C.: The Role of Particle Size, Ballast, Temperature, and Oxygen in the Sinking Flux to the Deep Sea, Global Biogeochemical Cycles, 32, 858–876, https://doi.org/10.1029/2017GB005710, https://agupubs.onlinelibrary.wiley.com/doi/abs/10.1029/2017GB005710, 2018.

DeVries, T., Primeau, F., and Deutsch, C.: The sequestration efficiency of the biological pump, Geophysical Research Letters, 39, https://doi.org/10.1029/2012GL051963, http://dx.doi.org/10.1029/2012GL051963, l13601, 2012.

DeVries, T., Liang, J.-H., and Deutsch, C.: A mechanistic particle flux model applied to the oceanic phosphorus cycle, Biogeosciences, 11, 5381–5398, https://doi.org/10.5194/bg-11-5381-2014, http://www.biogeosciences.net/11/5381/2014/, 2014.

Duteil, O., Koeve, W., Oschlies, A., Bianchi, D., Galbraith, E., Kriest, I., and Matear, R.: A novel estimate of ocean oxygen utilisation points to a reduced rate of respiration in the ocean interior, Biogeosciences, 10, 7723–7738, https://doi.org/10.5194/bg-10-7723-2013, http://www.biogeosciences.net/10/7723/2013/, 2013.

Eggleston, S. and Galbraith, E. D.: The devil's in the disequilibrium: multi-component analysis of dissolved carbon and oxygen changes under a broad range of forcings in a general circulation model, Biogeosciences, 15, 3761–3777, https://doi.org/10.5194/bg-15-3761-2018, https://www.biogeosciences.net/15/3761/2018/, 2018.

Fay, A. R. and McKinley, G. A.: Global open-ocean biomes: mean and temporal variability, Earth System Science Data, 6, 273–284, https://doi.org/10.5194/essd-6-273-2014, http://www.earth-syst-sci-data.net/6/273/2014/, 2014.

Follows, M. J., Ito, T., and Dutkiewicz, S.: On the solution of the carbonate chemistry system in ocean biogeochemistry models, Ocean Modelling, 12, 290 – 301, https://doi.org/https://doi.org/10.1016/j.ocemod.2005.05.004, http://www.sciencedirect.com/science/article/pii/S1463500305000533, 2006.

Garcia, H. E., Locarnini, R. A., Boyer, T. P., Antonov, J. I., Baranova, O. K., Zweng, M. M., Reagan, J. R., and Johnson, D. R.: World Ocean Atlas 2013, Volume 4: Dissolved Inorganic Nutrients (phosphate, nitrate, silicate)., in: NOAA Atlas NESDIS, edited by Levitus, S., U.S. Government Printing Office, Washington, D.C., 2014.

Gloor, M., Gruber, N., Hughes, T. M. C., and Sarmiento, J. L.: Estimating net air-sea fluxes from ocean bulk data: Methodology and application to the heat cycle, Global Biogeochemical Cycles, 15, 767–782, https://doi.org/10.1029/2000GB001301, http://dx.doi.org/10.1029/2000GB001301, 2001.

Guidi, L., Legendre, L., Reygondeau, G., Uitz, J., Stemmann, L., and Henson, S. A.: A new look at ocean carbon remineralization for estimating deepwater sequestration, Global Biogeochemical Cycles, pp. n/a–n/a, https://doi.org/10.1002/2014GB005063, http://dx.doi.org/10.1002/2014GB005063, 2014GB005063, 2015.

Henson, S., Sanders, R., and Madsen, E.: Global patterns in efficiency of particulate organic carbon export and transfer to the deep ocean, Global Biogeochemical Cycles, 26, GB1028, https://doi.org/10.1029/2011GB004099, 2012.

Henson, S. A., Sarmiento, J. L., Dunne, J. P., Bopp, L., Lima, I., Doney, S. C., John, J., and Beaulieu, C.: Detection of anthropogenic climate change in satellite records of ocean chlorophyll and productivity, Biogeosciences, 7, 621–640, https://doi.org/10.5194/bg-7-621-2010, http://www.biogeosciences.net/7/621/2010/, 2010.

Henson, S. A., Sanders, R., Madsen, E., Morris, P. J., Le Moigne, F., and Quartly, G. D.: A reduced estimate of the strength of the ocean's biological carbon pump, Geophysical Research Letters, 38, L04 606, https://doi.org/10.1029/2011GL046735, http://dx.doi.org/10.1029/2011GL046735, 2011.

Hülse, D., Arndt, S., Wilson, J. D., Munhoven, G., and Ridgwell, A.: Understanding the causes and consequences of past marine carbon cycling variability through models, Earth-Science Reviews, 171, 349 – 382, https://doi.org/https://doi.org/10.1016/j.earscirev.2017.06.004, http://www.sciencedirect.com/science/article/pii/S0012825216303191, 2017.

Ito, T. and Follows, M. J.: Preformed phosphate, soft-tissue pump and atmospheric CO_2, Journal of Marine Research, 64, 813 – 839, 2005.

John, E., Wilson, J., Pearson, P., and Ridgwell, A.: Temperature-dependent remineralization and carbon cycling in the warm Eocene oceans, Palaeogeography, Palaeoclimatology, Palaeoecology, 413, 158 – 166, https://doi.org/http://dx.doi.org/10.1016/j.palaeo.2014.05.019, http://www.sciencedirect.com/science/article/pii/S0031018214002685, 2014.

Jokulsdottir, T. and Archer, D.: A stochastic, Lagrangian model of sinking biogenic aggregates in the ocean (SLAMS 1.0): model formulation, validation and sensitivity, Geoscientific Model Development, 9, 1455–1476, https://doi.org/10.5194/gmd-9-1455-2016, http://www.geosci-model-dev.net/9/1455/2016/, 2016.

Khatiwala, S.: A computational framework for simulation of biogeochemical tracers in the ocean, Global Biogeochemical Cycles, 21, GB3001, https://doi.org/10.1029/2007GB002923, http://dx.doi.org/10.1029/2007GB002923, 2007.

Khatiwala, S., Visbeck, M., and Cane, M. A.: Accelerated simulation of passive tracers in ocean circulation models, Ocean Modelling, 9, 51 – 69, https://doi.org/http://dx.doi.org/10.1016/j.ocemod.2004.04.002, http://www.sciencedirect.com/science/article/pii/S1463500304000307, 2005.

Khatiwala, S., Primeau, F., and Holze, M.: Ventilation of the deep ocean constrained with tracer observations and implications for radiocarbon estimates of ideal mean age, Earth and Planetary Science Letters, 325-326, 116 – 125, https://doi.org/doi:10.1016/j.epsl.2012.01.038, http://www.sciencedirect.com/science/article/pii/S0012821X12000672, 2012.

Kirtman, B., Power, S., Adedoyin, J., Boer, G., Bojariu, R., Camilloni, I., Doblas-Reyes, F., Fiore, A., Kimoto, M., Meehl, G., Prather, M., Sarr, A., Schar, C., Sutton, R., van Oldenborgh, G., Vecchi, G., and Wang, H.: Near-term Climate Change: Projections and Predictability, in: Climate Change 2013: The Physical Science Basis. Contribution of Working Group I to the Fifth Assessment Report of the Intergovernmental Panel on Climate Change, edited by Stocker, T., Qin, D., Plattner, G.-K., Tignor, M., Allen, S., Boschung, J., Nauels, A., Xia, Y., Bex, V., and Midgley, P., Cambridge University Press, http://www.ipcc.ch/report/ar5/wg1/, 2013.

Kriest, I. and Oschlies, A.: On the treatment of particulate organic matter sinking in large-scale models of marine biogeochemical cycles, Biogeosciences, 5, 55–72, https://doi.org/10.5194/bg-5-55-2008, http://www.biogeosciences.net/5/55/2008/, 2008.

Kriest, I. and Oschlies, A.: MOPS-1.0: towards a model for the regulation of the global oceanic nitrogen budget by marine biogeochemical processes, Geoscientific Model Development, 8, 2929–2957, https://doi.org/10.5194/gmd-8-2929-2015, http://www.geosci-model-dev.net/8/2929/2015/, 2015.

Kriest, I., Oschlies, A., and Khatiwala, S.: Sensitivity analysis of simple global marine biogeochemical models, Global Biogeochemical Cycles, 26, GB2029, https://doi.org/10.1029/2011GB004072, http://dx.doi.org/10.1029/2011GB004072, 2012.

Kwon, E. Y., Primeau, F., and Sarmiento, J. L.: The impact of remineralization depth on the air-sea carbon balance, Nature Geoscience, 2, 630–635, http://dx.doi.org/10.1038/ngeo612, 2009.

Lam, P. J., Doney, S. C., and Bishop, J. K. B.: The dynamic ocean biological pump: Insights from a global compilation of particulate organic carbon, $CaCO_3$, and opal concentration profiles from the mesopelagic, Global Biogeochemical Cycles, 25, GB3009, https://doi.org/10.1029/2010GB003868, 2011.

Laufkötter, C., John, J. G., Stock, C. A., and Dunne, J. P.: Temperature and oxygen dependence of the remineralization of organic matter, Global Biogeochemical Cycles, 31, 1038–1050, https://doi.org/10.1002/2017GB005643, http://dx.doi.org/10.1002/2017GB005643, 2017GB005643, 2017.

Lefort, S., Aumont, O., Bopp, L., Arsouze, T., Gehlen, M., and Maury, O.: Spatial and body-size dependent response of marine pelagic communities to projected global climate change, Global Change Biology, 21, 154–164, https://doi.org/10.1111/gcb.12679, http://dx.doi.org/10.1111/gcb.12679, 2015.

Longhurst, A.: Ecological Geography of the Sea, Academic Press, San Diego, 1998.

Marinov, I., Gnanadesikan, A., Sarmiento, J. L., Toggweiler, J. R., Follows, M., and Mignone, B. K.: Impact of oceanic circulation on biological carbon storage in the ocean and atmospheric pCO_2, Global Biogeochemical Cycles, 22, GB3007, https://doi.org/10.1029/2007GB002958, http://dx.doi.org/10.1029/2007GB002958, 2008.

Marsay, C., Sanders, R., Henson, S., Pabortsava, K., Achterberg, E., and Lampitt, R.: Attenuation of sinking particulate organic carbon flux through the mesopelagic ocean, Proceedings of the National Academy of Sciences, 112, 1089–1094, https://doi.org/10.1073/pnas.1415311112, http://www.pnas.org/content/112/4/1089.abstract, 2015.

Martin, J., Knauer, G., Karl, D., and Broenkow, W.: VERTEX: carbon cycling in the northeast Pacific, Deep Sea Research, 43, 267 – 285, 1987.

McKay, M. D., Beckman, R. J., and Conover, W. J.: A Comparison of Three Methods for Selecting Values of Input Variables in the Analysis of Output From a Computer Code, Technometrics, 21, 239 – 245, 1979.

Meyer, K. M., Ridgwell, A., and Payne, J. L.: The influence of the biological pump on ocean chemistry: implications for long-term trends in marine redox chemistry, the global carbon cycle, and marine animal ecosystems, Geobiology, 14, 207–219, https://doi.org/10.1111/gbi.12176, http://dx.doi.org/10.1111/gbi.12176, 2016.

Mikaloff Fletcher, S. E., Gruber, N., Jacobson, A. R., Doney, S. C., Dutkiewicz, S., Gerber, M., Follows, M., Joos, F., Lindsay, K., Menemenlis, D., Mouchet, A., Müller, S. A., and Sarmiento, J. L.: Inverse estimates of anthropogenic CO_2 uptake, transport, and storage by the ocean, Global Biogeochemical Cycles, 20, GB2002, https://doi.org/10.1029/2005GB002530, http://dx.doi.org/10.1029/2005GB002530, 2006.

Najjar, R. G., Jin, X., Louanchi, F., Aumont, O., Caldeira, K., Doney, S. C., Dutay, J.-C., Follows, M., Gruber, N., Joos, F., Lindsay, K., Maier-Reimer, E., Matear, R. J., Matsumoto, K., Monfray, P., Mouchet, A., Orr, J. C., Plattner, G.-K., Sarmiento, J. L., Schlitzer, R., Slater, R. D., Weirig, M.-F., Yamanaka, Y., and Yool, A.: Impact of circulation on export production, dissolved organic matter, and dissolved oxygen in the ocean: Results from Phase II of the Ocean Carbon-cycle Model Intercomparison Project (OCMIP-2), Global Biogeochemical Cycles, 21, GB3007, https://doi.org/10.1029/2006GB002857, http://dx.doi.org/10.1029/2006GB002857, 2007.

Orr, J. C., Fabry, V. J., Aumont, O., Bopp, L., Doney, S. C., Feely, R. A., Gnanadesikan, A., Gruber, N., Ishida, A., Joos, F., Key, R. M., Lindsay, K., Maier-Reimer, E., Matear, R., Monfray, P., Mouchet, A., Najjar, R. G., Plattner, G.-K., Rodgers, K. B., Sabine, C. L., Sarmiento, J. L., Schlitzer, R., Slater, R. D., Totterdell, I. J., Weirig, M.-F., Yamanaka, Y., and Yool, A.: Anthropogenic ocean acidification over the twenty-first century and its impact on calcifying organisms, Nature, 437, 681–686, https://doi.org/10.1038/nature04095, 2005.

Orr, J. C., Najjar, R. G., Aumont, O., Bopp, L., Bullister, J. L., Danabasoglu, G., Doney, S. C., Dunne, J. P., Dutay, J.-C., Graven, H., Griffies, S. M., John, J. G., Joos, F., Levin, I., Lindsay, K., Matear, R. J., McKinley, G. A., Mouchet, A., Oschlies, A., Romanou, A., Schlitzer, R., Tagliabue, A., Tanhua, T., and Yool, A.: Biogeochemical protocols and diagnostics for the CMIP6 Ocean Model Intercomparison Project (OMIP), Geoscientific Model Development, 10, 2169–2199, https://doi.org/10.5194/gmd-10-2169-2017, https://www.geosci-model-dev.net/10/2169/2017/, 2017.

Pasquier, B. and Holzer, M.: The plumbing of the global biological pump: Efficiency control through leaks, pathways, and time scales, Journal of Geophysical Research: Oceans, 121, 6367–6388, https://doi.org/10.1002/2016JC011821, https://agupubs.onlinelibrary.wiley.com/doi/abs/10.1002/2016JC011821, 2016.

Pianosi, F., Beven, K., Freer, J., Hall, J. W., Rougier, J., Stephenson, D. B., and Wagener, T.: Sensitivity analysis of environmental models: A systematic review with practical workflow, Environmental Modelling & Software, 79, 214 – 232, https://doi.org/http://dx.doi.org/10.1016/j.envsoft.2016.02.008, http://www.sciencedirect.com/science/article/pii/S1364815216300287, 2016.

Riebesell, U., Kortzinger, A., and Oschlies, A.: Sensitivities of marine carbon fluxes to ocean change, Proceedings of the National Academy of Sciences of the United States of America, 106, 20 602–20 609, https://doi.org/10.1073/pnas.0813291106, 2009.

Roth, R., Ritz, S. P., and Joos, F.: Burial-nutrient feedbacks amplify the sensitivity of atmospheric carbon dioxide to changes in organic matter remineralisation, Earth System Dynamics, 5, 321–343, https://doi.org/10.5194/esd-5-321-2014, http://www.earth-syst-dynam.net/5/321/2014/, 2014.

Sarmiento, J. L., Slater, R., Barber, R., Bopp, L., Doney, S. C., Hirst, A. C., Kleypas, J., Matear, R., Mikolajewicz, U., Monfray, P., Soldatov, V., Spall, S. A., and Stouffer, R.: Response of ocean ecosystems to climate warming, Global Biogeochemical Cycles, 18, GB3003, https://doi.org/10.1029/2003GB002134, http://dx.doi.org/10.1029/2003GB002134, 2004.

Segschneider, J. and Bendtsen, J.: Temperature-dependent remineralization in a warming ocean increases surface pCO_2 through changes in marine ecosystem composition, Global Biogeochemical Cycles, 27, 1214–1225, https://doi.org/10.1002/2013GB004684, http://dx.doi.org/10.1002/2013GB004684, 2013.

Sigman, D. M., Hain, M. P., and Haug, G. H.: The polar ocean and glacial cycles in atmospheric CO_2 concentration, Nature, 466, 47–55, http://dx.doi.org/10.1038/nature09149, 2010.

Weber, T., Cram, J., Leung, S., DeVries, T., and Deutsch, C.: Deep ocean nutrients imply large latitudinal variation in particle transfer efficiency, Proceedings of the National Academy of Sciences, 113, 8606 – 611, 2016.

Yamamoto, A., Abe-Ouchi, A., and Yamanaka, Y.: Long-term response of oceanic carbon uptake to global warming via physical and biological pumps, Biogeosciences, 15, 4163–4180, https://doi.org/10.5194/bg-15-4163-2018, https://www.biogeosciences.net/15/4163/2018/, 2018.

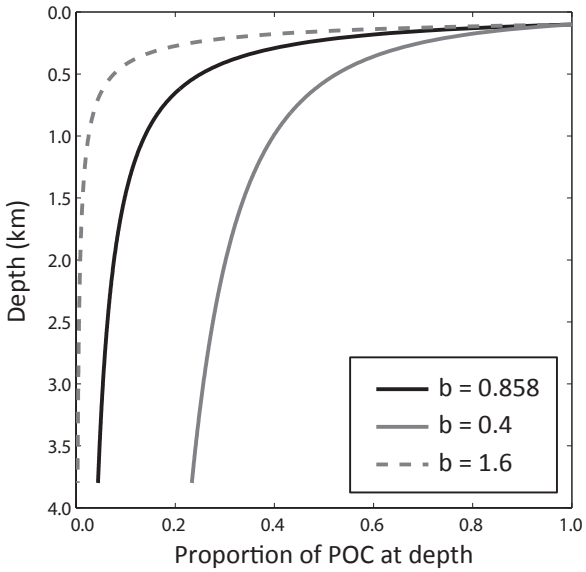

Figure 1. The normalised water column distribution of particulate fluxes defined using the Martin curve. As a comparison, Martin curves are shown with the exponent found by Martin et al. (1987) (b=0.858) and minimum and maximum exponent values used in this study based on sediment trap data compilations (b=0.4, b=1.6 Henson et al., 2012; Marsay et al., 2015; Guidi et al., 2015). All curves have export depth (z_0, eqn. 1) of 120 m.

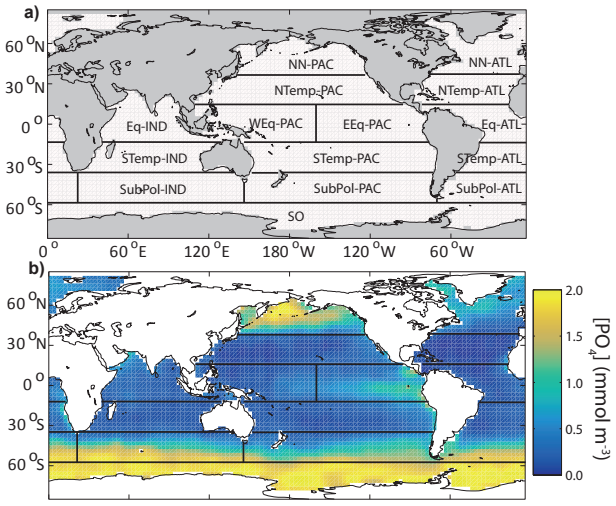

Figure 2. a) Location and names of the 15 regions defined on the model grid based on Gloor et al. (2001). Boundaries are at 58°S, 36°S, 13°S, 13°N, and 36°N. The equatorial Pacific is split at 98.75°E following Mikaloff Fletcher et al. (2006). Each region can be assigned a value of b that is independent of other regions. b) Location of regions superimposed on the annual mean surface $[PO_4]$ from World Ocean Atlas 13 (Garcia et al., 2014) regridded to the model grid.

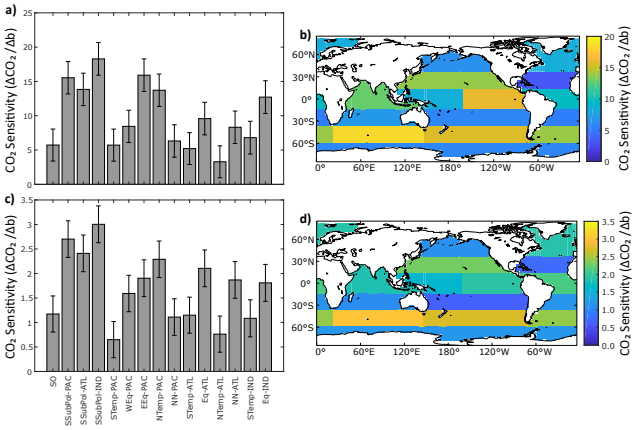

Figure 3. Regional sensitivity ($\Delta CO_2/\Delta b$) of atmospheric CO_2 (ppm) to changes in Martin curves for the constant-export scheme (panels a & b) and restoring-uptake scheme (panels c & d).The sensitivity value reflects the increase in CO_2 (preformed PO_4) for an increase in b (shallower remineralisation). Errorbars in panels a & c are 95% confidence intervals for the linear regression coefficients. Atmospheric CO_2 is inferred from modelled preformed PO_4 using empirical relationships in Figure A1.

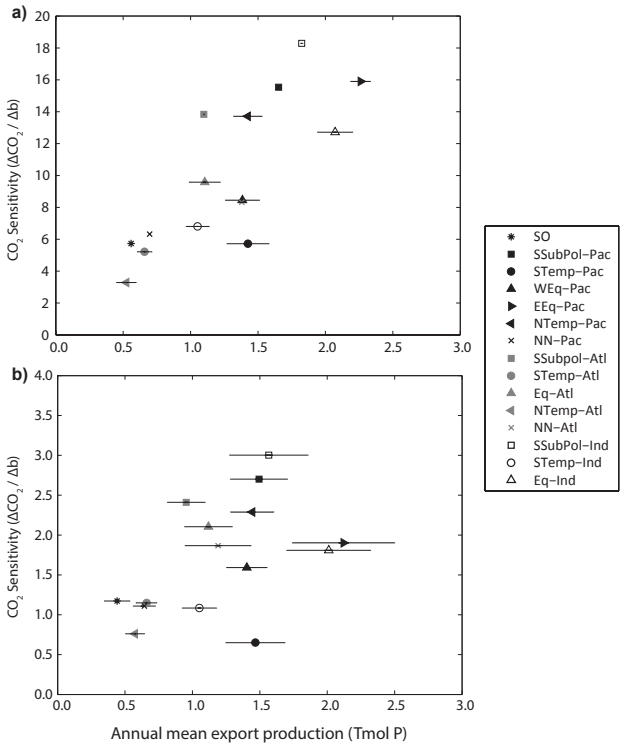

Figure 4. Relationship between regional CO_2 sensitivity and annual export of PO_4 in each region using (a) the constant-export scheme and (b) the restoring-uptake scheme. Annual export is shown as the mean of the 200 ensemble experiments with ± 1 standard deviation error bars.

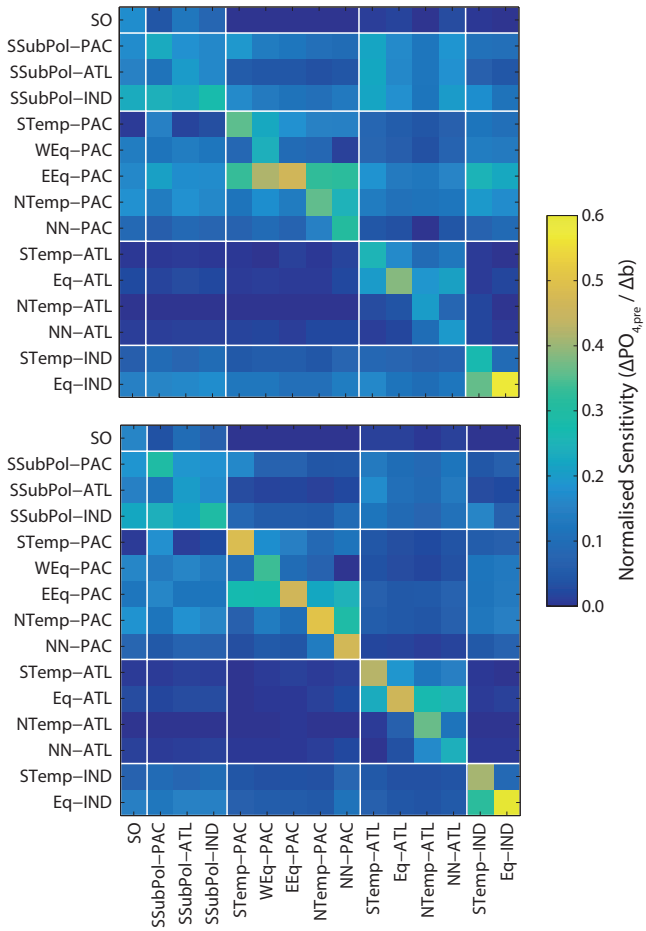

Figure 5. Sensitivity of steady-state normalised mean preformed [PO_4] exported from each region ($\overline{[P_{pre}^{region}]}$ | $\overline{[\hat{P}_{pre}^{region}]}$). $\overline{[P_{pre}^{region}]}$ | $\overline{[\hat{P}_{pre}^{region}]}$ from each region is expressed as a function of b using linear regression. $\overline{[P_{pre}^{region}]}$ is normalised to the range of values within each region in the ensemble to account for large differences in preformed $\overline{[P_{pre}^{region}]}$ between regions. The regression coefficients are arranged such that each row shows the impact of changing b in that region on $\overline{[P_{pre}^{region}]}$ | $\overline{[\hat{P}_{pre}^{region}]}$ across other regions. The upper and lower panels show the results for the constant-export and restoring-uptake schemes respectively.

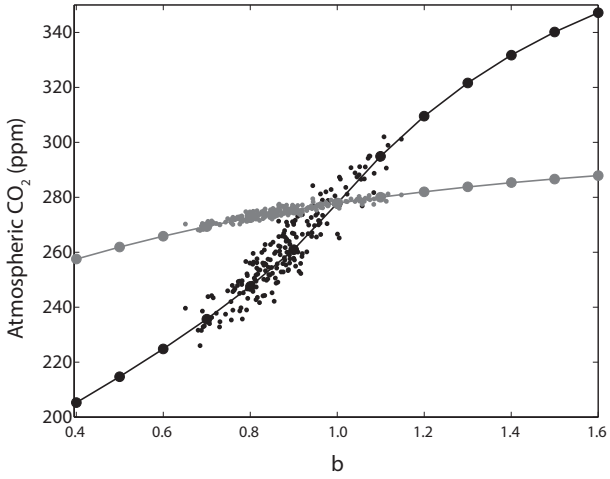

Figure 6. Comparison of CO_2 sensitivity when b is varied as globally uniform parameter (solid lines) and when b is varied regionally in the Latin hypercube samples and calculated as an area-weighted geometric mean of e-folding depths converted back to b to correct for non-linearities in the Martin Curve. Runs using the constant-export scheme are shown in black and restoring-uptake runs are shown in grey.

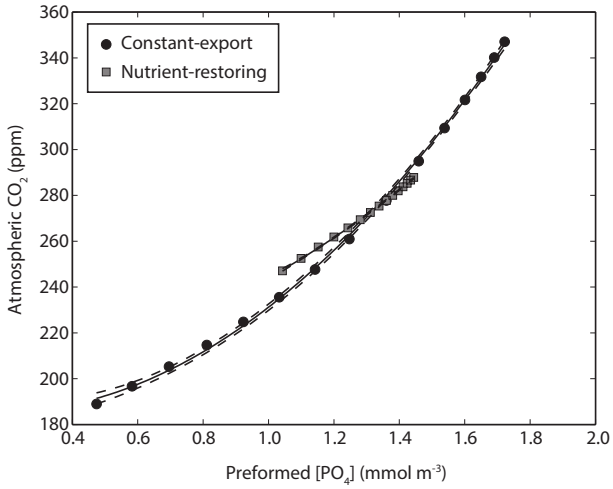

Figure A1. Relationship between preformed PO_4 and atmospheric CO_2 in the biogeochemical model using nutrient-restoring and constant-export when the Martin curve is varied globally between 0.4 and 1.6. A quadratic function ($\Delta CO_2 = \beta_1 \Delta {PO_4}_{,pre}{}^2 + \beta_2 \Delta PO_{4,pre} + \beta_3$) is fitted to the combined data with non-linear least squares is shown with 95 % confidence intervals. The coefficients for the two fits are β_1=66.59, β_2=-22.48 and β_3=187.09 for constant-export and β_1=42.80, β_2=-6.69 and β_3=207.95 for restoring-uptake.

Table 1. Key metrics and sensitivity estimates for each region and basins. Representative metrics including area (% of global area), region-integrated mean annual POP export (% of global POP export), and mean preformed [PO_4] (% of global mean) are taken from the control run. CO_2 sensitivity estimates for both the restoring-uptake and constant-export ensembles given as $\Delta CO_2/\Delta b$ ~~)~~(β_k from eqn. 2) with 95% confidence intervals and as a % ($\beta_k/\sum_k \beta_k$).

	Control			Constant Export		Restoring Uptake	
	Area (%)	POP Export (%)	$PO_{4,pre}$ (%)	β_k ($\Delta CO_2/\Delta b$)	$\beta_k/\sum_k \beta_k$ (%)	β_k ($\Delta CO_2/\Delta b$)	$\beta_k/\sum_k \beta_k$ (%)
SO	6.70	2.81	40.20	5.73±2.33	3.83	1.17±0.37	4.58
SubPol-PAC	7.67	8.35	5.23	15.54±2.36	10.40	2.70±0.37	10.55
STemp-PAC	10.37	7.86	0.29	5.72±2.34	3.83	0.65±0.37	2.54
Weq-PAC	7.21	7.46	0.11	8.45±2.35	5.66	1.59±0.37	6.22
Eeq-PAC	8.20	11.53	0.24	15.91±2.37	10.64	1.90±0.38	7.43
Ntemp-PAC	9.69	7.66	0.26	13.72±2.36	9.18	2.29±0.37	8.94
NN-PAC	4.94	3.50	4.21	6.32±2.36	4.23	1.11±0.37	4.33
SubPol-ATL	4.84	5.52	12.22	13.84±2.37	9.26	2.41±0.37	9.41
Stemp-ATL	4.46	3.53	0.14	5.21±2.32	3.49	1.15±0.37	4.49
Eq-ATL	5.45	6.06	0.10	9.58±2.37	6.41	2.10±0.37	8.22
NTemp-ATL	5.13	3.09	0.04	3.29±2.33	2.20	0.76±0.37	2.97
NN-ATL	4.84	7.04	23.54	8.32±2.37	5.57	1.87±0.37	7.29
SubPol-IND	6.86	9.18	13.04	18.29±2.38	12.24	3.00±0.38	11.73
STemp-IND	6.31	5.63	0.20	6.80±2.39	4.55	1.08±0.38	4.23
Eq-IND	7.32	10.85	0.20	12.72±2.38	8.51	1.81±0.38	7.06
>38°S[a]	26.08	25.85	70.68	53.40	35.73	9.29	36.27
Subantarctic[b]	19.38	23.04	30.48	47.67	31.90	8.11	31.69
Pacific	40.41	37.96	5.11	50.11	33.54	7.54	29.46
Atlantic	19.88	19.72	23.81	26.40	17.67	5.88	22.97
Indian	13.63	16.48	0.40	19.52	13.06	2.89	11.30

[a] For comparison with Southern Ocean estimate defined as >40°S in Kwon et al. (2009) [b] SubPol-PAC, SubPol-ATL and SubPol-IND